Characterizing the Lipkin-Meshkov-Glick model excited state quantum phase transition using dynamical and statistical properties of the diagonal entropy

Qian Wang
Department of Physics, Zhejiang Normal University, Jinhua 321004, China and
CAMTP-Center for Applied Mathematics and Theoretical Physics,
University of Maribor, Mladinska 3, SI-2000 Maribor, Slovenia

Francisco Pérez-Bernal
Departamento de Ciencias Integradas y Centro de Estudios Avanzados en Física,
Matemáticas y Computación, Universidad de Huelva, Huelva 21071, Spain and
Instituto Carlos I de Física Teórica y Computacional, Universidad de Granada, Granada 18071, Spain
(Dated: March 25, 2021)

Using the diagonal entropy, we analyze the dynamical signatures of the Lipkin-Meshkov-Glick (LMG) model excited-state quantum phase transition (ESQPT). We first show that the time evolution of the diagonal entropy behaves as an efficient indicator of the presence of an ESQPT. We also compute the probability distribution of the diagonal entropy values over a certain time interval and we find that the resulting distribution provides a clear distinction between the different phases of ESQPT. Moreover, we observe that the probability distribution of the diagonal entropy at the ESQPT critical point has a universal form, well described by a beta distribution, and that a reliable detection of the ESQPT can be obtained from the diagonal entropy central moments.

I. INTRODUCTION

The notion of excited-state quantum phase transition (ESQPT) [1, 2] was first introduced to describe the non-analytical properties in excited states of quantum systems and was soon identified, both theoretically [3–10] and experimentally [11–16], in various many-body systems. For a recently published review on the subject, see Ref. [17]. Being a generalization of ground-state quantum phase transitions (QPTs) [18, 19], ESQPTs are manifested by the appearance of a singularity in the density of states -or in one of its derivatives- at a critical energy value, for fixed Hamiltonian parameters [17, 20]. It has been found that ESQPTs play an important role in several contexts, including quantum decoherence processes [21–23], quantum chaos [24–27], and quantum thermodynamics [28, 29]. Many efforts have been devoted to understanding the intriguing static [20, 30–36] and dynamic [37–46] properties of this new type of phase transition.

Motivated by the recent advances on experimental techniques, the study of nonequilibrium dynamics of isolated quantum systems has received much attention in the past few years [47–50]. Along this direction, it is natural and important to explore how ESQPTs influence nonequilibrium dynamics of isolated systems. To date, several remarkable dynamical effects of ESQPTs have been revealed: an enhanced survival probability decay [41–43, 45, 51], an exponential growth of out-of-time-order correlators [52], and singularities in the time evolution of observables [38]. Moreover, the investigation of how to dynamically probe ESQPTs is also under an active development [10, 23, 37, 39, 45, 46] and implies possible ways of experimental exploration of ESQPTs through their evidences in the dynamics of isolated quantum many-body systems. In spite of these many works, quite a few aspects of the dynamical signatures of ESQPTs are still under discussion and more works are required in order to get a deeper understanding of the properties of ESQPTs.

In this work, we consider the Lipkin-Meshkov-Glick (LMG) model [53–55] and study the dynamical features of its ESQPT by means of the diagonal entropy. The diagonal entropy, for a given set of energy eigenstates, is defined as $\mathcal{S}_d = -\sum_n \rho_{nn} \ln \rho_{nn}$, where ρ_{nn} are the diagonal elements of the density matrix ρ in the basis of energy eigenstates [56]. This definition connects this quantity with the Shannon information entropy of the probability distribution corresponding to the energy eigenbasis [46]. The diagonal entropy exhibits most of the properties of a thermodynamic entropy, including additivity. Hence, it remains constant in adiabatic processes and it increases when systems are taken out of equilibrium. That makes the diagonal entropy a fine option for the study of nonequilibrium dynamics in isolated quantum [57–62]. Moreover, $\mathcal{S}_d$ is consistent with the well-known von Neumann's entropy for systems in equilibrium. It is also worth mentioning that, since the diagonal entropy only involves the diagonal part of the density matrix, in principle it can be experimentally accessed [61].

In the present work, we first focus on the time evolution of the diagonal entropy in a cyclic quench. We show that the time evolution of the diagonal entropy reveals the ESQPT existence displaying qualitatively distinct dynamics in the different ESQPT phases. Then, we investigate the probability distribution of the diagonal entropy values over a certain time interval. We show how the underlying ESQPT determines the distribution statistical properties. In particular, at the ESQPT critical energy, the diagonal entropy probability distribution has a universal form, independent of the system size and the Hamiltonian parameter values, that is in good agreement with the beta distribution. We also show that it

is possible to detect the ESQPT from the values of the central moments of the diagonal entropy probability distribution.

The article is structured as follows. In Sec. II, we describe the protocol used in this work and introduce the LMG model, briefly reviewing its main properties. In Sec. III, we present our main results and discuss how the signatures of ESQPT can be identified in the dynamics of the diagonal entropy as well as its statistical properties. Finally, we summarize the main conclusions of this work in Sec. IV.

II. PROTOCOL AND MODEL

A. Protocol and diagonal entropy

Assuming the system under study is described by a Hamiltonian $H(g)$, with g being a control parameter, we consider a cycle protocol with sudden changes of the control parameter at two different times. As depicted in Fig. 1(a), the protocol consists of the following processes. (i) Initially, the control parameter value is g_i, the Hamiltonian is H_i, and the system is in the state $\rho_n^{(i)} = |\psi_n^{(i)}\rangle\langle\psi_n^{(i)}|$, where $|\psi_n^{(i)}\rangle$ is the n-th H_i eigenstate, with eigenvalue $E_n^{(i)}$. (ii) At time $t = 0$, the control parameter is suddenly changed (quenched) from the initial value g_i to a final value g_f and the Hamiltonian of the system is a new one, H_f, with eigenstates $|\psi_n^{(f)}\rangle$ and eigenvalues $E_n^{(f)}$. From $t = 0$ on, the dynamics of the system is governed by the Hamiltonian H_f. (iii) At time $t = \tau$, the system undergoes a second quench, which changes the control parameter from g_f back to its initial value g_i, completing the cycle protocol. From now on, the system evolves under H_i for $t \geq \tau$.

The state of the system at $t = \tau$ is given by $\rho_\tau = e^{-iH_f\tau}\rho_n^{(i)}e^{iH_f\tau}$ and, therefore, the diagonal entropy at $t = \tau$ in the basis of eigenstates of the H_i Hamiltonian can be written as

$$\mathcal{S}_d(\tau) = -\sum_k \mathcal{C}_k(\tau)\ln\mathcal{C}_k(\tau), \tag{1}$$

where $\mathcal{C}_k(\tau) = |\langle\psi_k^{(i)}|e^{-iH_f\tau}|\psi_n^{(i)}\rangle|^2$ and $|\psi_k^{(i)}\rangle$ is the k-th eigenstates of Hamiltonian H_i [58]. As already mentioned, it has been argued that the diagonal entropy fulfills the second law of thermodynamics, namely, it grows when a system is taken out of equilibrium, it saturates at the equilibration time scale, it is an additive quantity, and it is conserved for adiabatic processes [56, 57]. Note that $\mathcal{C}_k(\tau)$ is equal to the well-known survival probability when we take $k = n$ and that, independently of τ and H_f values, $\sum_k \mathcal{C}_k(\tau) = 1$.

The diagonal entropy is a non-linear function of the density matrix and, therefore, the long-time averaged diagonal entropy, denoted as $\overline{\mathcal{S}_d(\tau)}$, is not equal to the diagonal entropy for the long-time averaged state, $\langle\mathcal{S}_d\rangle$ [58, 63]. It has been conjectured that for a pure initial state, the deviation between these two quantities, Δ, satisfies the inequality $\Delta = \langle\mathcal{S}_d\rangle - \overline{\mathcal{S}_d(\tau)} \leq 1 - \gamma$, where $\gamma = 0.5772\ldots$ is the Euler's constant [63]. As Δ fluctuations are minimal once the system is in equilibrium, it has been employed to explore the connection between relaxation and transitions between integrability and chaos in various quantum systems [58, 59]. In the present work, we pay heed to the ESQPT signatures in the nonequilibrium dynamics of a quantum isolated system, investigating the dynamical and statistical properties of the diagonal entropy of the LMG model, in which the above mentioned cycle protocol is implemented.

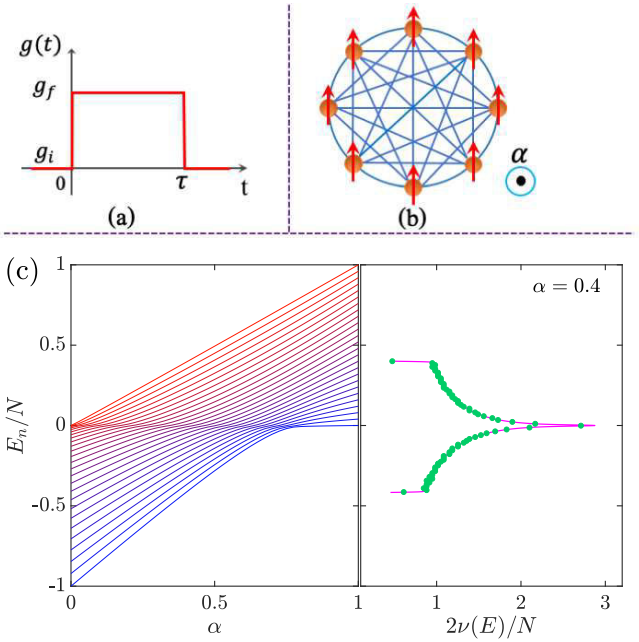

FIG. 1. (a) The quench protocol studied in this work, as described in the text. (b) Schematic representation of the LMG model. Spins are fully connected through an infinite range coupling and in an external magnetic field with strength α along the z direction. (c) Rescaled even-parity energy spectrum of the Lipkin model as a function of α with $N = 50$ (left panel) and the rescaled density of states of the LMG model for $\alpha = 0.4$ with $N = 5000$ (right panel). The green dots denote the numerical results, while the solid line is obtained via Eq. (3). All quantities are dimensionless.

B. Lipkin-Meshkov-Glick (LMG) model

The LMG model, originally introduced as a toy model in nuclear physics [53–55], was later found to be useful in many areas of physics [28, 52, 64–68] and has been realized with high precision in different experimental platforms [69–72]. In particular, it has been used as a paradigmatic model in the study of ESQPTs[2, 21–23, 29, 30, 39, 43]. This model can be mapped to the transverse Ising model with infinite-range interactions.

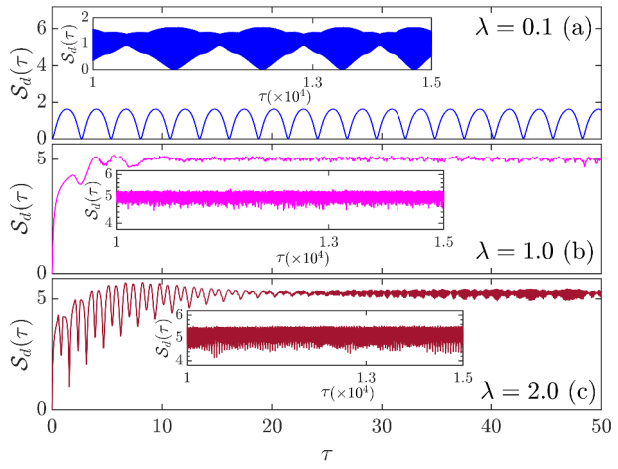

FIG. 2. Time evolution of $\mathcal{S}_d(\tau)$ for three different values of λ, with control parameter $\alpha = 0.4$ and system size $N = 1000$. The inset in each panel shows the long time behavior of $\mathcal{S}_d(\tau)$ with τ in a range from 10^4 to 1.5×10^4 for the corresponding λ values. The axes in all figures are dimensionless.

Hence, the LMG model describes N fully connected 1/2-spin particles coupled to an external transverse field with strength α; see Fig. 1(b) for a schematic representation of the LMG model.

Employing the collective spin operators $J_\beta = \sum_l \sigma_\beta^l/2$, where $\beta = \{x, y, z\}$ and σ_β^l are Pauli spin matrices for the l-th spin, the Hamiltonian of the LMG model can be written as

$$H = -\frac{4(1-\alpha)}{N} J_x^2 + \alpha \left(J_z + \frac{N}{2} \right), \tag{2}$$

where N is the total number of spins and the control parameter $\alpha \in [0, 1]$ is the strength of the magnetic field along the z direction. For simplicity's sake, we consider $\hbar = 1$ throughout this work and set the quantities studied in this article as dimensionless.

The Hamiltonian in Eq. (2) conserves the total spin $\mathbf{J}^2 = J_x^2 + J_y^2 + J_z^2$, whose eigenvalues are $j(j+1)$ with $0 \leq j \leq N/2$. We perform our calculations in the sector of maximum angular momentum, $j = N/2$, with dimension $N + 1$. Moreover, as the parity operator $\Pi = e^{i\pi(J_z + j)}$ also commutes with H, the Hamiltonian matrix in $j = N/2$ sector can be further split into two blocks, an even parity block, with dimension $N/2 + 1$, and an odd parity block, with dimension $N/2$. We further restrict our calculations to the even parity block, which includes the system ground state.

The elements of the Hamiltonian matrix in the basis of eigenstates of J_z, $|j, m_z\rangle$, with $-N/2 \leq m_z \leq N/2$, are given by

$$\langle j, m_z | H | j, m_z \rangle = q_\alpha \left(\frac{N}{2} + m_z \right) + \alpha - 1,$$

$$\langle j, m_z + 2 | H | j, m_z \rangle = -\frac{1-\alpha}{N} \sqrt{\left(\frac{N}{2} - m_z - 1 \right)} \sqrt{\left(\frac{N}{2} - m_z \right) \left(\frac{N}{2} + m_z + 1 \right) \left(\frac{N}{2} + m_z + 2 \right)},$$

where $q_\alpha = [2(1-\alpha)m_z/N] + 2\alpha - 1$.

The LMG Hamiltonian in Eq. (2) undergoes a second-order ground state quantum phase transition at the critical point $\alpha_c = 0.8$ [73, 74]. The system is in the broken-symmetry phase when $\alpha < \alpha_c$ and in the symmetric phase for $\alpha \geq \alpha_c$. Another remarkable feature of the LMG model is the occurrence of an ESQPT for $\alpha < \alpha_c$ [2, 21, 22, 44]. ESQPTs in systems with a single effective degree of freedom, like the LMG model, are characterized by a high density of excited levels at a critical energy value, E_c. The level density is nonanalytical in the mean field limit (large N limit) of the system [17]. This is illustrated for the LMG model in the left panel of Fig. 1(c), where it is clear how energy levels are piling up the neighborhood of the critical energy $E_c = 0$.

The eigenvalues clustering at $E_c = 0$ leads to a cusp singularity in the density of states, $\nu(E)$, defined as $\nu(E) = \sum_n \delta(E - E_n)$. In the semiclassical limit $N \to \infty$, $\nu(E)$ can be analytically calculated as [22, 23]

$$\nu(E) = \frac{N}{2\pi} \int \delta[E - \mathcal{H}_{cl}(x, p)] dx dp, \tag{3}$$

where $\mathcal{H}_{cl}$ is the classical counterpart of H in Eq. (2). The right panel of Fig. 1(c) plots the density of states for the case of $\alpha = 0.4$ with $N = 5000$. We observe that $\nu(E)$ obtained by means of Eq. (3) has an excellent agreement with the numerical data and it is evident the expected cusp divergence at $E_c = 0$. In the following, we focus on the identification of the signatures of this ESQPT in the dynamical and statistical properties of the diagonal entropy.

III. THE LMG MODEL DIAGONAL ENTROPY

In the first hand, we focus on the dynamics of the diagonal entropy $\mathcal{S}_d(\tau)$, and in the second hand, we consider

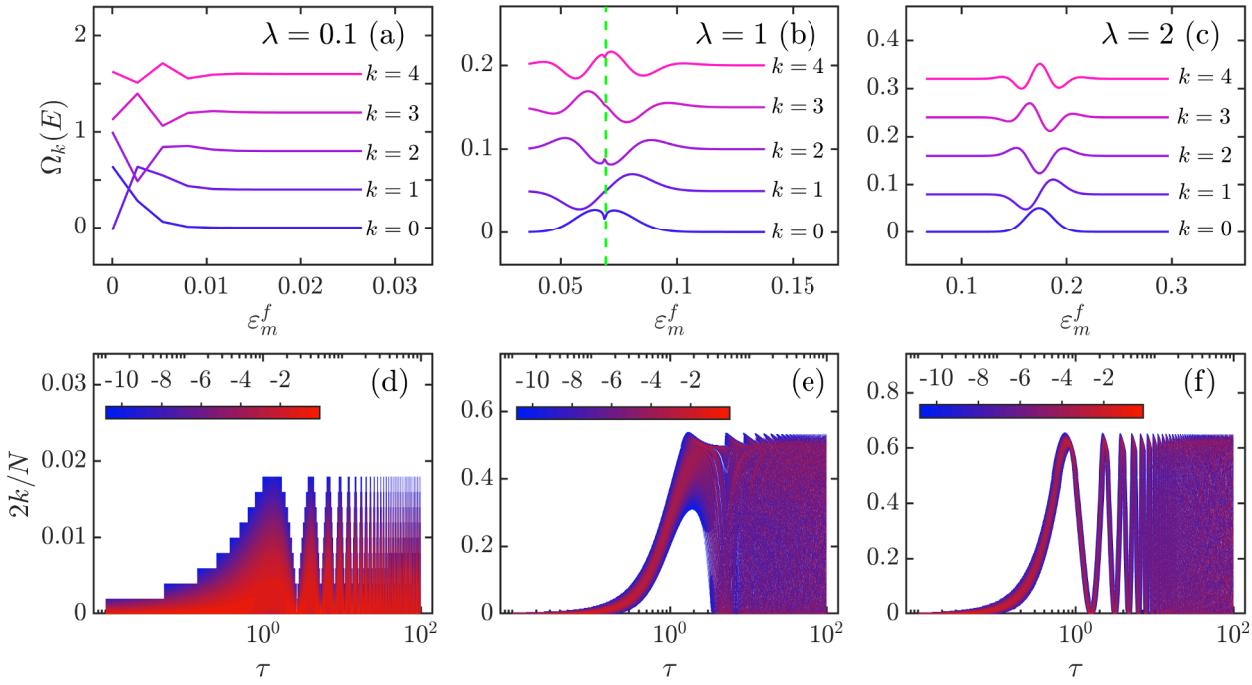

FIG. 3. Panels (a)-(c): $\Omega_k(E)$ as a function of the rescaled energy for the first 5 eigenstates ($k = 0, 1, \ldots, 4$) with $\lambda = 0.1, 1, 2$. The rescaled energy is defined as $\varepsilon_m^f = [E_m^{(f)} - E_0^{(f)}]/[E_{max}^{(f)} - E_0^{(f)}]$, where $E_0^{(f)}$ is the ground state energy of H_f, while $E_{max}^{(f)}$ denotes the maximum energy of H_f. To offer a three-dimensional-like visualization, the different $\Omega_k(E)$ curves are shifted in the y-direction by $0.4k$ (a), $0.05k$ (b), and $0.08k$ (c). The green dashed line in panel (b) indicates the rescaled ESQPT critical energy. Panels (d)-(f): Heat map plot depicting $\ln[\mathcal{C}_k(\tau)]$ as a function of k and τ for the same values of λ as in panels (a)-(c). White color indicates $\mathcal{C}_k(\tau) = 0$. In all cases the control parameter $\alpha = 0.4$ and the system size is $N = 1000$. All quantities are dimensionless.

the distribution of values of $\mathcal{S}_d(\tau)$ with $\tau \geq 0$. We are mainly interested in how the ESQPT affects the time evolution of $\mathcal{S}_d(\tau)$ and the $\mathcal{S}_d(\tau)$ probability distribution, as well as the moments of this distribution.

In our study, the above described cycle protocol is achieved as follows. Initially, the system is at the ground state, $|\psi_0^{(i)}\rangle$, of Hamiltonian (2) with $H_i = H$, $g_i = 0$, and $\rho_0^{(i)} = |\psi_0^{(i)}\rangle\langle\psi_0^{(i)}|$. At time $t = 0$, we turn on an external magnetic field along the z direction with strength λ. We thus have $g_f = \lambda$ and $H_f = H + \lambda(J_z + N/2)$. The external magnetic field is then switched off at time $t = \tau$ to back to the starting point, completing the closed cycle. The diagonal entropy at time $t = \tau$, $\mathcal{S}_d(\tau)$, is given by Eq. (1) with

$$\mathcal{C}_k(\tau) = |\langle\psi_k^{(i)}|e^{-iH_f\tau}|\psi_0^{(i)}\rangle|^2 = \left|\int dE\Omega_k(E)e^{-iE\tau}\right|^2. \tag{4}$$

Here, $|\psi_k^{(i)}\rangle$ is the kth eigenstate of H in Eq. (2) and

$$\Omega_k(E) = \sum_m \langle\psi_k^{(i)}|\psi_m^{(f)}\rangle\langle\psi_m^{(f)}|\psi_0^{(i)}\rangle\delta[E - E_m^{(f)}], \tag{5}$$

with $|\psi_m^{(f)}\rangle$ denotes the mth eigenstate of H_f corresponding to the eigenvalue $E_m^{(f)}$. We point out that results qualitatively similar to the reported ones are obtained for different choices of the initial state.

The system can be driven through the critical energy of ESQPT by varying the strength of the external magnetic field, λ. We define the critical strength, denoted as λ_c^α, as the magnetic field intensity that brings the system, initially in the ground state, to the critical energy, $E_c = 0$. In the LMG model case this critical strength can be obtained using the semiclassical approach [21, 22]

$$\lambda_c^\alpha = \frac{1}{2}(4 - 5\alpha), \tag{6}$$

where $\alpha \in (0, 4/5)$. We would like to point out that the ESQPT critical strength, λ_c^α, differs from the critical strength for the ground state quantum phase transition, λ_{c0}^α[22].

A. Dynamical behavior of $\mathcal{S}_d(\tau)$

As a starting point, we investigate the signatures of the ESQPT in the dynamics of the LMG diagonal entropy. In Fig. 2, the diagonal entropy is depicted as a function of τ, $\mathcal{S}_d(\tau)$, for three different values of λ. In all

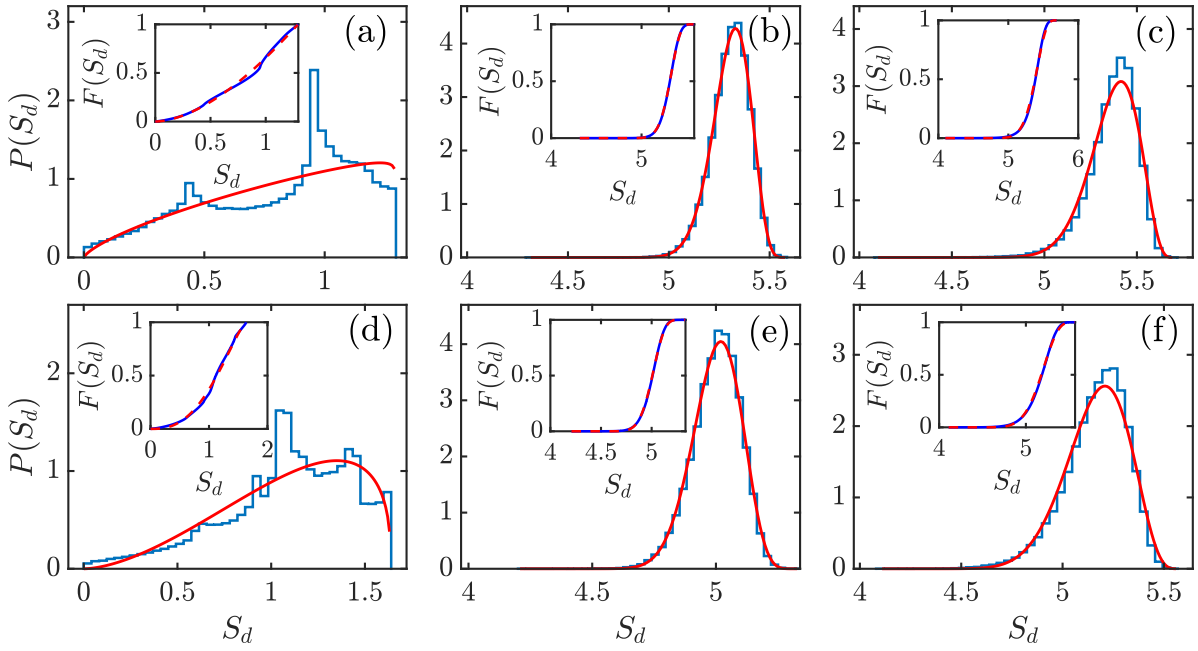

FIG. 4. Panels (a)-(c): Probability distribution of the diagonal entropy $P(S_d)$ for $\lambda = 0.1$ (a), $\lambda = \lambda_c^\alpha = 1.5$ (b), and $\lambda = 2$ (c). The control parameter is fixed to $\alpha = 0.2$. Panels (d)-(f): Probability distribution of the diagonal entropy $P(S_d)$ for $\lambda = 0.1$ (a), $\lambda = \lambda_c^\alpha = 1$ (b), and $\lambda = 2$ with $\alpha = 0.4$. In all cases the system size is $N = 1000$. The red solid line in each panel denotes the corresponding optimized beta distribution from Eq. (9). The parameter values (a, b, S_0, S_m) are (a) $(1.722, 1.038, 0, 1.295)$, (b) $(23.705, 6.637, 4.316, 5.582)$, (c) $(18.172, 4.638, 4.101, 5.692)$, (d) $(2.697, 1.362, 0, 1.64)$, (e) $(18.972, 7.964, 4.208, 5.334)$, (f) $(12.292, 4.676, 4.109, 5.567)$. The inset in each panel shows with a blue solid line the cumulative distribution function of the diagonal entropy $F(S_d)$ and the corresponding result for the beta distribution (red dashed line), respectively. All quantities are dimensionless.

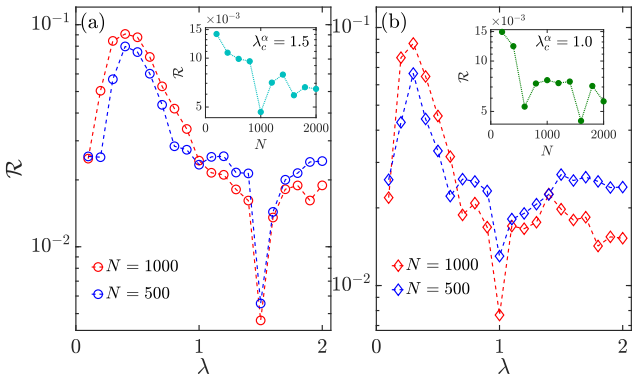

FIG. 5. $\mathcal{R}$ in Eq. (11) as a function of λ for different system size $N = 500$ and 1000, with control parameter values $\alpha = 0.2$ (a) and $\alpha = 0.4$ (b). The inset in (a) shows $\mathcal{R}$ as a function of system size N for $\alpha = 0.2$ and $\lambda_c^\alpha = 1.5$, while the inset in (b) plots $\mathcal{R}$ as a function of N for $\alpha = 0.4$ and $\lambda_c^\alpha = 1.0$. The axes in all figures are dimensionless.

cases the control parameter $\alpha = 0.4$ and the system size $N = 1000$. In this case, according to Eq. (6), we have $\lambda_c^\alpha = 1$. From Fig. 2, it is clear that the behavior of $\mathcal{S}_d(\tau)$ as a function of τ strongly depends on the λ value. Specifically, for $\lambda < \lambda_c^\alpha$, $\mathcal{S}_d(\tau)$ periodically oscillates around a small value, as shown in Fig. 2(a). Increasing λ leads to an increase in the $\mathcal{S}_d(\tau)$ value while the initially regular oscillations gradually change towards an irregular pattern. As can be seen from Fig. 2(b), once $\lambda = \lambda_c^\alpha = 1$, $\mathcal{S}_d(\tau)$ displays a fast growth which rapidly saturates at a maximum value with tiny fluctuations. Notice that the suppression of the oscillating behavior has also been found in the survival probability dynamics [51]. As it is shown in Refs. [51, 75], this feature stems from the fact that eigenstates having different structure are dynamically entangled at the ESQPT critical energy. Above the critical point, e.g. the $\lambda = 2$ case depicted in Fig. 2(c), we observe that $\mathcal{S}_d(\tau)$ increases with time, with larger oscillations, until it irregularly oscillates around the same saturation value as in the previous case.

The observed features in the dynamics of the diagonal entropy indicate that the underlying system ESQPT has a strong impact on the equilibration process of the quenched system. Obviously, these features can be used to detect the existence of an ESQPT, through the singular behavior of $\mathcal{S}_d(\tau)$ at $\lambda = \lambda_c^\alpha$. Moreover, different phases of an ESQPT can also be identified by the distinct behaviors of the diagonal entropy for $\lambda < \lambda_c^\alpha$ and $\lambda > \lambda_c^\alpha$, respectively.

To understand the features exhibited by $\mathcal{S}_d(\tau)$, we note

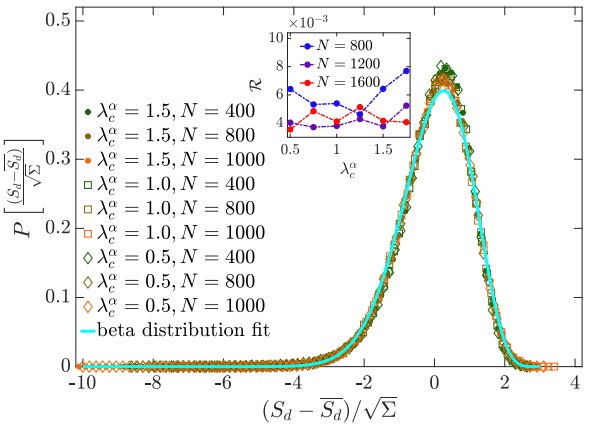

FIG. 6. Probability distribution of the shifted and rescaled diagonal entropy, i. e., $(S_d - \overline{S_d})/\sqrt{\Sigma}$, at different λ_c^α and for several system sizes, N. Here, $\overline{S_d}$ denotes the averaged S_d, and Σ is the variance of S_d. The cyan solid line denotes the fitted beta distribution [cf. Eq. (9)] with fitting parameters (a, b, S_0, S_m) given by $(22.308, 6.692, -10, 3)$. Inset: The RMSE, $\mathcal{R}$, between $P[(S_d - \overline{S_d})/\sqrt{\Sigma}]$ and the fitted beta distribution as a function of λ_c^α for different system sizes, N. The axes in all figures are dimensionless.

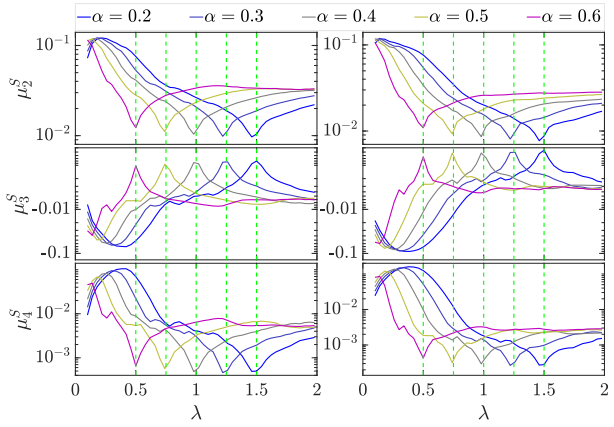

FIG. 7. Second, third, and fourth central moments (as labelled) of $P(S_d)$ as a function of λ for $\alpha = 0.2, 0.3, \ldots, 0.6$ and a system size value $N = 500$ (left column) and $N = 1000$ (right column). The vertical dashed lines in each panel mark the critical values λ_c^α for each corresponding α. The axes in all figures are dimensionless.

that, as indicated in Eq. (4), $\mathcal{C}_k(\tau)$ is the square modulus of the Fourier transform of $\Omega_k(E)$, defined in Eq. (5). Therefore, the remarkably different dependence of τ for the $\mathcal{S}_d(\tau)$ depicted in the different panels of Fig. 2 stems from the change of the $\Omega_k(E)$ properties as the system straddles through the ESQPT. The behavior of $\mathcal{S}_d(\tau)$ at the critical energy of the ESQPT can be explained from the $\Omega_k(E)$ singular structure. To cast light upon this particular point, we plot $\Omega_k(E)$ and the corresponding $\mathcal{C}_k(\tau)$ in Fig. 3. For the sake of comparison use the same λ values than in Fig. 2 and, again, a control parameter value $\alpha = 0.4$ and a system size $N = 1000$.

For the case of $\lambda = 0.1 < \lambda_c^\alpha$, as shown in Fig. 3(a), nonzero $\Omega_k(E)$ values are rather localized at low H_f eigenenergies and the main contribution is due to states with $k \leq 3$. The simple structure of $\Omega_k(E)$ in this case explains the oscillations in τ of $\mathcal{C}_k(\tau)$, that occur for small k values, with $\mathcal{C}_k(\tau) = 0$ for other values of k, as it is illustrated in Fig. 3(d). This implies that $\mathcal{S}_d(\tau)$ is a periodic function of τ as shown in Fig. 2(a). As λ increases, the number of states contributing to $\Omega_k(E)$ increases, involving states with larger k values. This, in turn, involves an increase in the $\mathcal{S}_d(\tau)$ value. Once the critical point $\lambda = \lambda_c^\alpha = 1$ is explored, we obtain the results plotted in Fig. 3(b). As the involved values of k are larger, the complexity of $\Omega_k(E)$ increases. However, in this particular case, a most remarkable feature of $\Omega_k(E)$ is the cusp-like shape near the ESQPT critical energy (marked in Fig. 3(b) by a light green dashed line), occurring at all k values. As shown in Ref. [41], the same cusp-like structure in $\Omega_0(E)$ leads to a fast decay of the survival probability, $\mathcal{C}_0(\tau)$, followed by random oscillations with tiny amplitude. In the present work, we find that cusps in $\Omega_k(E)$ for nonzero k have the same effect on the time evolution of the correspondent $\mathcal{C}_k(\tau)$, as illustrated in Fig. 3(e). Therefore, the behavior of $\mathcal{S}_d(\tau)$ at $\lambda = \lambda_c^\alpha$ can be traced back to the cusp-like structures in $\Omega_k(E)$ at the critical energy of ESQPT. When $\lambda = 2 > \lambda_c^\alpha$, the structure of $\Omega_k(E)$ at small values of k are regular, whereas as k increases the structures of $\Omega_k(E)$ become more and more complex, in a similar way to the case in Fig. 3(d). As a consequence, the behavior of $\mathcal{C}_k(\tau)$ is initially regular, followed by small irregular oscillations with $\mathcal{C}_k(\tau) \approx 0$ [see Fig. 3(f)]. This explains the slow growth of $\mathcal{S}_d(t)$ at times close to zero for the $\lambda = 2$ case [see Fig. 2(c)].

These results strongly indicate that the LMG model ESQPT has a very significant impact on the equilibration processes that follow a quench. Therefore, the time dependent behavior of the diagonal entropy can be used to reliably distinguish among the different phases of the ESQPT. In addition to this, at the critical point, the particular dynamical behavior of the diagonal entropy acts as a good indicator of the presence of ESQPT.

B. Statistical properties of $\mathcal{S}_d(\tau)$

In this subsection we explore the statistical properties of the diagonal entropy to gain further insight on how the ESQPT influences the nonequilibrium dynamics of the LMG model after the quantum quench. To this end, we investigate the distribution of values of the diagonal entropy in a long-time interval, considering the probability

distribution of $\mathcal{S}_d(\tau)$ values in a time window $[\tau_0, \tau_0+\Delta\tau]$

$$P(S_d) = \lim_{\Delta\tau\to\infty} \frac{1}{\Delta\tau} \int_{\tau_0}^{\tau_0+\Delta\tau} \delta[\mathcal{S}_d(\tau) - S_d]d\tau, \quad (7)$$

where the value of τ_0 is much larger than the initial time scale. The correct calculation of this distribution function implies the consideration of all the $\mathcal{S}_d(\tau)$ intricacies (see, e. g. the insets in Fig. 2); which means that we need to evolve the system for a long period of time. In our simulation, we take $\tau_0 = \Delta\tau = 10^4$. We have carefully checked that the results obtained for larger τ_0 and $\Delta\tau$ values do not modify the present conclusions. The cumulative distribution function of S_d is given by

$$F(S_d) = \int_{S_0}^{S_d} P(x)dx, \quad (8)$$

where S_0 is the minimal value of the distribution range and $P(x)$ is the probability distribution function in Eq. (7).

In Fig. 4, we plot the computed probability distribution of the diagonal entropy and the corresponding cumulative distribution for two values of the control parameter, $\alpha = 0.2$ [panels (a)-(c)] and $\alpha = 0.4$ [panels (d)-(f)] with a system size, $N = 1000$. In both cases, we include values of λ below, at, and above the critical value λ_c^α. From this figure it can be observed that $P(S_d)$ is a doubly peaked distribution at low λ values, due to the periodic oscillations in $\mathcal{S}_d(\tau)$. Meanwhile, the small amplitude of the $\mathcal{S}_d(\tau)$ oscillations is translated to nonzero values of $P(S_d)$ at low values of S_d. As λ value increases, the growing in $\mathcal{S}_d(\tau)$ shifts $P(S_d)$ towards higher values of S_d. We further observe that the increase in λ also transforms $P(S_d)$ from a double-peaked form to an asymmetric bell shape structure. This stems from the fact that the greater the λ value, the larger the random oscillations of $\mathcal{S}_d(\tau)$ at long times.

Further understanding of the properties of $P(S_d)$ can be gained by noting that the values of the diagonal entropy in a certain time window are limited to an interval of finite length and $P(S_d)$ has different shapes at different values of λ. These facts, together with the results presented by one of us that concern the modeling of the statistical distribution of Shannon entropy values [76], led us to fit the $P(S_d)$ values by a beta distribution, defined as [77–79]

$$\varphi_B(x) = \frac{(x - S_0)^{a-1}(S_m - x)^{b-1}}{(S_m - S_0)^{a+b-1}\mathcal{B}(a, b)}, \quad (9)$$

where S_m denotes the maximal value of the distribution range, a, b are the shape parameters of the distribution, and $\mathcal{B}(a, b) = \int_0^1 u^{a-1}(1 - u)^{b-1}du$ is the beta function. The cumulative distribution function of the beta distribution is given by

$$\Phi_B(x) = \int_{S_0}^{x} \varphi_B(y)dy, \quad (10)$$

where x is such that $S_0 \le x \le S_m$.

In Fig. 4, the fitted beta distribution in Eq. (9) and its cumulative distribution for each case are denoted by a red solid line in the main panel and a red dashed line in the inset. One can immediately identify the obvious deviation between $P(S_d)$ and the beta distribution when the value of λ is far away from the critical value λ_c^α, in particular for low λ values, as can be seen in the first and last columns of Fig. 4. However, at the critical point, with $\lambda = \lambda_c^\alpha$, the beta distribution agrees extremely well with the numerical results, as illustrated in panels (b) and (e) of Fig. 4. To quantitatively examine the differences between $P(S_d)$ and the beta distribution, we employ the root mean square error (RMSE), which quantifies the deviation between predicted and observed values [80]. For our purpose, we consider the RMSE, denoted by $\mathcal{R}$, between the cumulative distribution function of the diagonal entropy and the fitted beta distribution

$$\mathcal{R} = \sqrt{\left(\frac{1}{S_m - S_0}\right) \int_{S_0}^{S_m} [F(z) - \Phi_B(z)]^2 dz}, \quad (11)$$

where $F(z)$ and $\Phi_B(z)$ are given by Eqs. (8) and (10), respectively.

In Fig. 5, we plot the dependence of $\mathcal{R}$ with λ for different system sizes and for $\alpha = 0.2$ and 0.4. $\mathcal{R}$ shows an obvious dip at the critical value λ_c^α, and the minimum value decreases for increasing system size N. Therefore, the best agreement of $P(S_d)$ with the beta distribution occurs at the critical point of the ESQPT, as already shown in Fig. 4. Moreover, the agreement improves when increasing the system size, N. At the critical point, we further find that the decrease in $\mathcal{R}$ with the system size N is replaced by a tiny fluctuation around a vanishingly small value when $N > 1000$, regardless of the value of λ_c^α, as shown in the insets of Fig. 5.

The next question to address is whether the probability distribution of the diagonal entropy, $P(S_d)$, has an universal form at the critical point of ESQPT. In what follows, we show that this is indeed in our case. To this end, we standardize the probability distribution and consider a shifted and rescaled diagonal entropy, denoted by $\mathscr{S}_d$, defined as

$$\mathscr{S}_d = \frac{S_d - \overline{S_d}}{\sqrt{\Sigma}}, \quad (12)$$

where $\overline{S_d} = \int dS_d P(S_d) S_d$ is the averaged S_d and $\Sigma = \int dS_d P(S_d)(S_d - \overline{S_d})^2$ is the variance of S_d. We now investigate the probability distribution of $\mathscr{S}_d$, $P(\mathscr{S}_d)$, at different values of λ_c^α and for several system sizes N.

Our numerical results are shown in Fig. 6. We observe that numerical data for different λ_c^α and N collapse in a single distribution, indicating that $P(\mathscr{S}_d)$ is the universal distribution for the ESQPT. Moreover, the distribution $P(\mathscr{S}_d)$ can also be well fitted by the beta distribution in Eq. (9), with fitting parameters $(a, b, S_0, S_m) = (22.308, 6.692, -10, 3)$. The deviations between $P(\mathscr{S}_d)$

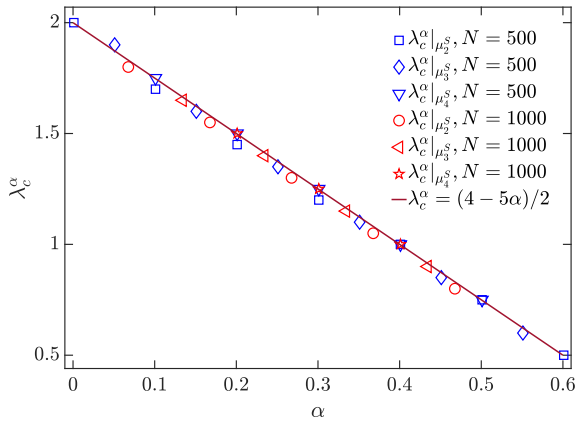

FIG. 8. Critical value λ_c^α, extracted from different central moments (as labelled), as a function of α for different system sizes N. For each central moment, the location of its extreme value has been identified as the critical value λ_c^α. The solid line denotes the analytical result, which gives by Eq. (6). The axes in the figure are dimensionless.

and the fitted beta distribution are vanishingly small at different λ_c^α and are also almost independent of the system size, N, as depicted in the inset of Fig. 6. This further confirms the universality of $P(\mathscr{S}_d)$ at the critical point of ESQPT.

Central moments of $P(S_d)$

Once defined the probability distribution of the diagonal entropy, we now turn to identify the signatures of the ESQPT in the statistical properties of $P(S_d)$, by investigating the central moments of $P(S_d)$. The n-th central moment of $P(S_d)$ is defined as

$$\mu_n^S = \mathbb{E}[(S_d - \overline{S_d})^n] = \int_{-\infty}^{+\infty} dS_d P(S_d)(S_d - \overline{S_d})^n. \quad (13)$$

The first central moment, μ_1^S, is always zero, thus we mainly focus on the moments with $n = 2, 3, 4$, the variance, skewness, and kurtosis of the distribution, respectively. These central moments provide information about the distribution shape.

In Fig. 7, we plot μ_2^S, μ_3^S and μ_4^S as a function of λ for different values of the α control parameter and the system size N. In this figure, it is evident that the three central moments have a non-analytic behavior, with cusps in the neighborhood of the λ_c^α critical values. Specifically, cusps in μ_2^S and μ_4^S display as minima that tend to zero as N increases. As the second and fourth central moments measure the fluctuations and the heaviness of the tail of a probability distribution, the minima values in μ_2^S and μ_4^S indicate that $P(S_d)$ has negligible fluctuations and becomes a light-tailed distribution in the vicinity of the ESQPT critical point, in accordance with the results observed in panels (b) and (e) of Fig. 4. The third central moment, μ_3^S, is always less than zero, independently of the values of the control parameter α and the system size N. It is known that the third central moment quantifies the distribution asymmetry. Therefore, negative μ_3^S values imply that the area under the left tail of $P(S_d)$ is larger than the one under the right tail, as shown in Fig. 4. For values of the control parameter $\lambda = \lambda_c^\alpha$, the third central moment μ_3^S shows a cusp-like dependence toward zero, which is sharper for larger values of N. This means that the system $P(S_d)$ distribution has its most symmetric shape at the ESQPT critical point, as can be seen in Figs. 4(b,e) and 6.

The different features displayed by the central moments of $P(S_d)$ suggest that for a given system the critical value of λ can be obtained numerically from the extreme, cusp-like, values of the central moments. By identifying the critical point as the location of the extreme values in the central moments, we have plotted the estimated λ_c^α as a function of α in Fig. 8. We also depict in the same figure the analytical result of λ_c^α from Eq. (6). As can be seen from the figure, numerical results show a good agreement with the analytical solution, in particular for the results from μ_3^S and μ_4^S. Moreover, the agreement can be enhanced increasing the system size. Therefore, we can confirm that the ESQPT has strong effects on the statistical properties of the probability distribution of the diagonal entropy, $P(S_d)$. Besides, the central moments of $P(S_d)$ can be used to reliably detect the critical point of the ESQPT.

IV. CONCLUSION

We have studied in detail the effects of the ESQPT on the dynamics and statistics of the diagonal entropy in a quantum many-body system, the LMG model, which undergoes an ESQPT at a certain critical energy. We have shown that the diagonal entropy exhibits a significant change in its time dependence as the system goes through the critical energy of the ESQPT. Hence, the existence of an ESQPT can be ascertained from the calculation of the dynamics of the diagonal entropy, which also allows us to efficiently distinguish between the different phases of the ESQPT. To understand the different dynamical behaviors of the diagonal entropy, we have explored the connections between the energy dependence of $\Omega_k(E)$ [cf. Eq. (5)] and the dynamics of the diagonal entropy. The results indicate the qualitative differences in time evolution of the diagonal entropy resulting from changes in $\Omega_k(E)$. In particular, at the critical energy of the ESQPT the diagonal entropy follows a very particular dynamics, that can be traced back to the highly nontrivial cusp structures in $\Omega_k(E)$.

The features observed in the dynamics of the diagonal entropy imply that the ESQPT has a significant influence on the probability distribution of the diagonal entropy. We have demonstrated that the distribution of the di-

agonal entropy transforms from a double peak form to an asymmetric bell shape, once the system crosses the ESQPT. In particular, we have found that the distribution of the diagonal entropy can be well described by a beta distribution at the critical point of the ESQPT. Hence, the distribution of the diagonal entropy can be considered as a useful tool for the ESQPT exploration. An intriguing and remarkable result of our study is the universal behavior exhibited by the distribution of the diagonal entropy at the critical point of ESQPT. We have confirmed that the distribution of the diagonal entropy values at the critical point is independent of both the system size and the control parameter value, and it is in good agreement with the beta distribution. Additionally, to examine more closely the effects of the ESQPT on the statistical properties of the diagonal entropy, we have analyzed the second, third, and fourth central moments of the diagonal entropy distribution. Our results suggest that the nonanalyticities in the central moments make them valid probes to identify the ESQPT critical point.

The universality of the diagonal entropy distribution at the critical point can be traced back to the nature of the diagonal entropy time dependence in the ESQPT, which stems from the cusps in the structure of $\Omega_k(E)$. We would like to emphasize that the same cusps have been found for ESQPTs in various systems [41, 51], which makes us expect that our results are robust and hold in other quantum many-body systems other than the LMG model, such as the Dicke model [3], the kicked-top model [5], and the Rabi model [6]. A very interesting topic for future work would be a systematic study of the statistical properties of the diagonal entropy in different many-body systems. The present results pave the way to a deeper understanding of ESQPT properties and shed light upon ESQPTs influence on the nonequilibrium dynamics of quantum systems. Moreover, we have also investigated the dynamical signatures of ESQPTs in classical phase space in one of our recent work [81]. Finally, the diagonal entropy measurement in quantum simulators is expected to be quite efficient [61], which make us believe that the obtained results could be experimentally verified in a near future.

ACKNOWLEDGMENTS

Q. W. acknowledges support from the National Science Foundation of China under Grant No. 11805165, Zhejiang Provincial Nature Science Foundation under Grant No. LY20A050001, and the Slovenian Research Agency (ARRS) under the Grants No. J1-9112 and No. P1-0306. FPB thanks the support of the Consejería de Conocimiento, Investigación y Universidades, Junta de Andalucía and European Regional Development Fund (ERDF) through projects SOMM17/6105/UGR and UHU-1262561 and the support of the Ministerio de Ciencia, Innovación y Universidades through project PID2019-104002GB-C21. Computing resources supporting this work were partly provided by the CEAFMC and Universidad de Huelva High Performance Computer (HPC@UHU) located in the Campus Universitario el Carmen and funded by FEDER/MINECO project UNHU-15CE-2848.

[1] P. Cejnar, M. Macek, S. Heinze, J. Jolie, and J. Dobeš, J. Phys. A: Math. Gen. **39**, L515 (2006).
[2] M. Caprio, P. Cejnar, and F. Iachello, Ann. Phys. (N. Y.) **323**, 1106 (2008).
[3] T. Brandes, Phys. Rev. E **88**, 032133 (2013).
[4] M. A. Bastarrachea-Magnani, S. Lerma-Hernández, and J. G. Hirsch, Phys. Rev. A **89**, 032101 (2014).
[5] V. M. Bastidas, P. Pérez-Fernández, M. Vogl, and T. Brandes, Phys. Rev. Lett. **112**, 140408 (2014).
[6] R. Puebla, M.-J. Hwang, and M. B. Plenio, Phys. Rev. A **94**, 023835 (2016).
[7] A. Relaño, C. Esebbag, and J. Dukelsky, Phys. Rev. E **94**, 052110 (2016).
[8] J. E. García-Ramos, P. Pérez-Fernández, and J. M. Arias, Phys. Rev. C **95**, 054326 (2017).
[9] Q.-W. Wang and S. Wu, Phys. Rev. A **102**, 063531 (2020).
[10] P. Feldmann, C. Klempt, A. Smerzi, L. Santos, and M. Gessner, "Excited-state quantum phase transitions in spinor bose-einstein condensates," (2020), arXiv:2011.02823 [cond-mat.quant-gas].
[11] D. Larese and F. Iachello, J. Mol. Struct. **1006**, 611 (2011).
[12] D. Larese, F. Pérez-Bernal, and F. Iachello, J. Mol. Struct. **1051**, 310 (2013).
[13] B. Dietz, F. Iachello, M. Miski-Oglu, N. Pietralla, A. Richter, L. von Smekal, and J. Wambach, Phys. Rev. B **88**, 104101 (2013).
[14] J. Khalouf-Rivera, M. Carvajal, L. F. Santos, and F. Pérez-Bernal, J. Phys. Chem. A **123**, 9544 (2019).
[15] T. Tian, H.-X. Yang, L.-Y. Qiu, H.-Y. Liang, Y.-B. Yang, Y. Xu, and L.-M. Duan, Phys. Rev. Lett. **124**, 043001 (2020).
[16] J. Khalouf-Rivera, F. Pérez-Bernal, and M. Carvajal, J. Quant. Spectrosc. and Rad. Transfer , 107436 (2020).
[17] P. Cejnar, P. Stránský, M. Macek, and M. Kloc, "Excited-state quantum phase transitions," (2021), arXiv:2011.01662 [quant-ph].
[18] L. Carr, *Understanding quantum phase transitions* (CRC press, 2010).
[19] S. Sachdev, *Quantum Phase Transitions* (Cambridge University Press, 2011).
[20] P. Stránský, M. Macek, and P. Cejnar, Ann. Phys. **345**, 73 (2014).
[21] A. Relaño, J. M. Arias, J. Dukelsky, J. E. García-Ramos, and P. Pérez-Fernández, Phys. Rev. A **78**, 060102 (2008).

[22] P. Pérez-Fernández, A. Relaño, J. M. Arias, J. Dukelsky, and J. E. García-Ramos, Phys. Rev. A **80**, 032111 (2009).
[23] Q. Wang and F. Pérez-Bernal, Phys. Rev. A **100**, 022118 (2019).
[24] P. Pérez-Fernández, A. Relaño, J. M. Arias, P. Cejnar, J. Dukelsky, and J. E. García-Ramos, Phys. Rev. E **83**, 046208 (2011).
[25] M. A. Bastarrachea-Magnani, S. Lerma-Hernández, and J. G. Hirsch, Phys. Rev. A **89**, 032102 (2014).
[26] M. A. Bastarrachea-Magnani, B. L. del Carpio, S. Lerma-Hernández, and J. G. Hirsch, Phys. Scr. **90**, 068015 (2015).
[27] C. M. Lóbez and A. Relaño, Phys. Rev. E **94**, 012140 (2016).
[28] R. Puebla and A. Relaño, Phys. Rev. E **92**, 012101 (2015).
[29] Q. Wang and H. T. Quan, Phys. Rev. E **96**, 032142 (2017).
[30] Z.-G. Yuan, P. Zhang, S.-S. Li, J. Jing, and L.-B. Kong, Phys. Rev. A **85**, 044102 (2012).
[31] R. Puebla and A. Relaño, EPL (Europhysics Letters) **104**, 50007 (2013).
[32] P. Stránský, M. Macek, A. Leviatan, and P. Cejnar, Ann. Phys. **356**, 57 (2015).
[33] P. Cejnar and P. Stránský, Phys. Lett. A **381**, 984 (2017).
[34] P. Pérez-Fernández and A. Relaño, Phys. Rev. E **96**, 012121 (2017).
[35] M. Šindelka, L. F. Santos, and N. Moiseyev, Phys. Rev. A **95**, 010103 (2017).
[36] M. Macek, P. Stránský, A. Leviatan, and P. Cejnar, Phys. Rev. C **99**, 064323 (2019).
[37] R. Puebla, A. Relaño, and J. Retamosa, Phys. Rev. A **87**, 023819 (2013).
[38] G. Engelhardt, V. M. Bastidas, W. Kopylov, and T. Brandes, Phys. Rev. A **91**, 013631 (2015).
[39] Q. Wang and F. Pérez-Bernal, Phys. Rev. A **100**, 062113 (2019).
[40] W. Kopylov, G. Schaller, and T. Brandes, Phys. Rev. E **96**, 012153 (2017).
[41] P. Pérez-Fernández, P. Cejnar, J. M. Arias, J. Dukelsky, J. E. García-Ramos, and A. Relaño, Phys. Rev. A **83**, 033802 (2011).
[42] L. F. Santos and F. Pérez-Bernal, Phys. Rev. A **92**, 050101 (2015).
[43] L. F. Santos, M. Távora, and F. Pérez-Bernal, Phys. Rev. A **94**, 012113 (2016).
[44] Q. Hummel, B. Geiger, J. D. Urbina, and K. Richter, Phys. Rev. Lett. **123**, 160401 (2019).
[45] F. Pérez-Bernal and L. F. Santos, Fortschr. Phys. **65**, 1600035 (2017).
[46] Z. Mzaouali, R. Puebla, J. Goold, M. E. Baz, and S. Campbell, "Work statistics and symmetry breaking in an excited state quantum phase transition," (2021), arXiv:2101.04985 [quant-ph].
[47] A. Polkovnikov, K. Sengupta, A. Silva, and M. Vengalattore, Rev. Mod. Phys. **83**, 863 (2011).
[48] T. Langen, R. Geiger, and J. Schmiedmayer, Annu. Rev. Condens. Matter Phys. **6**, 201 (2015).
[49] S. Bhattacharyya, S. Dasgupta, and A. Das, Sci. Rep **5**, 16490 (2015).
[50] A. Haldar, K. Mallayya, M. Heyl, F. Pollmann, M. Rigol, and A. Das, arXiv e-prints (2020), arXiv:2004.02905 [cond-mat.stat-mech].
[51] M. Kloc, P. Stránský, and P. Cejnar, Phys. Rev. A **98**, 013836 (2018).
[52] S. Pilatowsky-Cameo, J. Chávez-Carlos, M. A. Bastarrachea-Magnani, P. Stránský, S. Lerma-Hernández, L. F. Santos, and J. G. Hirsch, Phys. Rev. E **101**, 010202 (2020).
[53] H. Lipkin, N. Meshkov, and A. Glick, Nucl. Phys. **62**, 188 (1965).
[54] H. J. Lipkin, N. Meshkov, and A. J. Glick, Nucl. Phys. **62**, 199 (1965).
[55] H. J. Lipkin, N. Meshkov, and A. J. Glick, Nucl. Phys. **62**, 211 (1965).
[56] A. Polkovnikov, Ann. Phys. **326**, 486 (2011).
[57] L. F. Santos, A. Polkovnikov, and M. Rigol, Phys. Rev. Lett. **107**, 040601 (2011).
[58] I. García-Mata, A. J. Roncaglia, and D. A. Wisniacki, Phys. Rev. E **91**, 010902 (2015).
[59] O. Giraud and I. García-Mata, Phys. Rev. E **94**, 012122 (2016).
[60] E. J. Torres-Herrera and L. F. Santos, Ann. Phys. **529**, 1600284 (2017).
[61] Z.-H. Sun, J. Cui, and H. Fan, Phys. Rev. Research **2**, 013163 (2020).
[62] Z. Wang, Z.-H. Sun, Y. Zeng, H. Lang, Q. Hong, J. Cui, and H. Fan, Phys. Lett. A **384**, 126333 (2020).
[63] T. N. Ikeda, N. Sakumichi, A. Polkovnikov, and M. Ueda, Ann. Phys. **354**, 338 (2015).
[64] P. Ribeiro, J. Vidal, and R. Mosseri, Phys. Rev. Lett. **99**, 050402 (2007).
[65] F. de los Santos, E. Romera, and O. Castaños, Phys. Rev. A **91**, 043409 (2015).
[66] S. Campbell, G. De Chiara, M. Paternostro, G. M. Palma, and R. Fazio, Phys. Rev. Lett. **114**, 177206 (2015).
[67] A. Russomanno, F. Iemini, M. Dalmonte, and R. Fazio, Phys. Rev. B **95**, 214307 (2017).
[68] T. Xu, T. Scaffidi, and X. Cao, Phys. Rev. Lett. **124**, 140602 (2020).
[69] M. Albiez, R. Gati, J. Fölling, S. Hunsmann, M. Cristiani, and M. K. Oberthaler, Phys. Rev. Lett. **95**, 010402 (2005).
[70] T. Zibold, E. Nicklas, C. Gross, and M. K. Oberthaler, Phys. Rev. Lett. **105**, 204101 (2010).
[71] I. D. Leroux, M. H. Schleier-Smith, and V. Vuletić, Phys. Rev. Lett. **104**, 073602 (2010).
[72] V. Makhalov, T. Satoor, A. Evrard, T. Chalopin, R. Lopes, and S. Nascimbene, Phys. Rev. Lett. **123**, 120601 (2019).
[73] E. Romera, M. Calixto, and O. Castaños, Phys. Scripta **89**, 095103 (2014).
[74] O. Castaños, F. de los Santos, R. Yáñez, and E. Romera, Ann. Phys. **389**, 19 (2018).
[75] S. Lerma-Hernández, J. Chávez-Carlos, M. A. Bastarrachea-Magnani, L. F. Santos, and J. G. Hirsch, J. Phys. A: Math. Theor. **51**, 475302 (2018).
[76] Q. Wang and M. Robnik, Phys. Rev. E **102**, 032212 (2020).
[77] W. Feller, *An Introduction to Probability theory and its application Vol II* (John Wiley and Sons, 1971).
[78] N. L. Johnson, S. Kotz, and N. Balakrishnan, *Continuous univariate distributions* (John Wiley & Sons, Ltd, 1995).

[79] A. K. Gupta and S. Nadarajah, *Handbook of beta distribution and its applications* (CRC press, 2004).
[80] M. J. Schervish and M. DeGroot, *Probability and statistics* (Pearson Education, 2014).
[81] Q. Wang and F. Pérez-Bernal, arXiv e-prints , arXiv:2011.11932 (2020), arXiv:2011.11932 [quant-ph].